1995ApJ...448....8B

THE ASTROPHYSICAL JOURNAL, 448:8–16, 1995 July 20
© 1995. The American Astronomical Society. All rights reserved. Printed in U.S.A.

EFFECTS OF ATMOSPHERIC EMISSION ON GROUND-BASED MICROWAVE BACKGROUND MEASUREMENTS

M. BERSANELLI,[1] M. BENSADOUN,[2] L. DANESE,[3] G. DE AMICI,[2] A. KOGUT,[4] S. LEVIN,[5] M. LIMON,[2] D. MAINO,[1] G. F. SMOOT,[2] AND C. WITEBSKY[2]

Received 1994 October 21; accepted 1995 February 2

ABSTRACT

We present an analysis of multifrequency measurements of atmospheric emission in the Rayleigh-Jeans portion of the cosmic microwave background spectrum (1–90 GHz) taken since 1986 from White Mountain, CA, and from the South Pole. Correlations of simultaneous data at 10 and 90 GHz and accurate low-frequency measurements show good agreement with model predictions for both sites. Our data from the South Pole 1989 campaign combined with real-time measurements of the local atmospheric profiles provide accurate verification of the expected independent contributions of H_2O and O_2 emission. We show that variations on the order of 10% of the oxygen emission (both resonant and nonresonant components) are present on timescales of hours to days, mainly due to the evolution of the atmospheric pressure profile. Oxygen emission fluctuations appear larger than previously expected and may have significant consequences for ground-based cosmic microwave background experiments.

Subject headings: atmospheric effects — cosmic microwave background — Earth

1. INTRODUCTION

The emission from the Earth's atmosphere is the largest unwanted signal in most ground-based measurements of the cosmic microwave background (CMB), even when these are carried out from carefully selected, high-altitude sites. The substantial progress achieved in recent years in receiver performance increases the relative importance of the atmospheric foreground as a limiting factor in the quality of ground-based CMB results. Atmospheric effects strongly contribute to the uncertainty and poor data efficiency of both spectral (absolute) and anisotropy (differential) experiments. Beam switching at constant elevation is used in anisotropy experiments to cancel the atmospheric signal, but leaves atmospheric fluctuations as a dominant problem. For example, measurements in the 30–90 GHz range from the South Pole show that typically 70%–80% of the data must be rejected for excessive atmospheric fluctuations (Gaier et al. 1992; Meinhold et al. 1993; Lubin 1995), and it is very important to understand possible residual effects in the clear sky condition data actually used for CMB analysis. The effects of the atmospheric foreground also dominate the uncertainty of spectral measurements in the 2–90 GHz range (e.g., Bersanelli et al. 1994a, and references therein). Long-wavelength (>10 cm) measurements are hampered by strong Galactic synchrotron emission, and the uncertainties of the atmospheric and Galactic components are highly interrelated (e.g., De Amici et al. 1990; Bersanelli et al. 1994b). On the other hand, the obvious advantages of ground-based experiments over alternative solutions (balloon-borne or space) call for a quantitative assessment of atmospheric effects on CMB measurements, particularly from suitable sites and in clear-sky conditions.

Models for the propagation of millimeter and centimeter waves are discussed in the literature (e.g., Waters 1976; Liebe 1981; Danese & Partridge 1989; Ajello, Bonelli, & Sironi 1995). Model emission predictions require temperature, pressure, and water vapor density profiles and a description of continuum and lines spectra of O_2 and H_2O. These models rely heavily on data taken at or near the line centers and are extended with somewhat empirical extrapolations (Liebe 1984) to the low-emission windows exploited for astrophysical observations. Accurate radiometric data of the atmospheric emission in the line wings are necessary to verify the model predictions and constrain some of their parameters. However, only a few direct measurements have been performed.

As part of our campaigns to measure the low-frequency spectrum of the CMB we have collected since 1982 a large set of measurements of the atmospheric antenna temperature at various frequencies in the 1–90 GHz range from the White Mountain Barcroft Station, California (altitude 3800 m, latitude +37°.5; hereafter WM) and from the Amundsen-Scott South Pole Station, Antarctica (altitude 2830 m, latitude −90°; hereafter SP). The atmospheric data collected at WM before 1985 are discussed in Costales et al. (1986) and Smoot et al. (1987a). In this paper we discuss the new data and combine the multifrequency results from the two sites to test the theoretical model. We then analyze the time variation of atmospheric O_2 and H_2O emission and draw conclusions on the expected effects on CMB measurements.

2. THE ATMOSPHERIC MODEL

For a nonscattering and nonrefracting atmosphere in thermal equilibrium, the equation of transfer for a signal from outside the atmosphere in units of antenna temperature can be written (e.g., Waters 1976)

$$T(H_{\rm obs}) = T_\infty \exp\left[-\tau_\nu(0, s_{\rm obs})\right] + \int_0^{s_{\rm obs}} T_{\rm phys}(s') \exp\left[-\tau_\nu(s' - s_{\rm obs})\right] k_\nu(s')\, ds' , \quad (1)$$

[1] Istituto di Fisica Cosmica, Consiglio Nazionale delle Ricerche, via Bassini 15, 20133 Milano, Italy.
[2] Space Science Laboratory and Lawrence Berkeley Laboratory, M/S 50-205, University of California, Berkeley, CA 94720.
[3] SISSA—International School for Advanced Studies, Strada Costiera 11, 34014 Trieste, Italy.
[4] Hughes STX, Code 685, NASA/Goddard Space Flight Center, Greenbelt, MD 20771.
[5] Jet Propulsion Laboratory, California Institute of Technology, M/S 169-506, Pasadena, CA 91109.

© American Astronomical Society • Provided by the NASA Astrophysics Data System

1995ApJ...448....8B

where T_∞ is the antenna temperature of the background signal (in our case emission from the Galaxy, extragalactic sources, and the CMB), H_{obs} is the altitude of the observing site, $T_{phys} = c^2 B_\nu(T)/2k_B \nu^2$ with $B_\nu(T)$ the Planck function and k_B Boltzmann's constant [$T_{phys}(s')$ approaches the physical temperature at s' in the Rayleigh-Jeans approximation], and τ_ν and k_ν are, respectively, the optical depth and volume attenuation coefficient at frequency ν. The second term in equation (1) is the atmospheric antenna temperature, $T_{A,atm}$.

In order to determine the attenuation coefficients at a given observing site, the profiles of atmospheric temperature, pressure, and water vapor are required, as well as a parametric description of k_ν. Usually, standard profiles are adopted, which depend to first approximation on the latitude of the site (e.g., US Standard Atmosphere 1976). A complete description of lines and continuum attenuation coefficients of O_2 and H_2O can be found in Danese & Partridge (1989, hereafter D&P). By using all the published atmospheric data then available, D&P adjusted the reference model, based on Liebe (1985). The model optimization resulted in a 20% increase of the line strength of the 22.2 GHz H_2O line and a 15% increase of the strength of the 60 GHz O_2 line. Here we outline those features of the theoretical model which are directly constrained by radiometric measurements.

At low frequencies $T_{A,atm}$ is dominated by emission from the O_2 continuum, characterized by the attenuation coefficient (D&P):

$$(k_\nu)_{O_2,c} = \left(1.12 \times 10^{-4} p\theta^2 \frac{\gamma_0}{\gamma_0^2 + \nu^2} + 3.49 \times 10^{-11} p^2 \theta^{2.5}\right)\nu^2 , \quad (2)$$

where $\theta = 300/T(\mathrm{K})$ is the relative inverse temperature parameter, p (kPa) is the dry air pressure, and γ_0 (GHz) is the width parameter for the O_2 continuum. The latter can be represented as follows:

$$\gamma_0 = a(p + 1.1e)\theta^b , \quad (3)$$

where e (kPa) is the partial water vapor pressure; the parameters a (GHz kPa^{-1}) and b (adimensional) determine through equations (2) and (3) the amplitude of the O_2 continuum emission. The parameters a and b are directly constrained by low-frequency results.

At frequencies above ~ 10 GHz, in addition to O_2 emission, the contribution of water vapor becomes important. In the limit $\tau_\nu \ll 1$ from the second term on the right-hand side of equation (1) we can express the atmospheric temperature as (Partridge et al. 1984)

$$T_{A,atm}(\nu) = T_{A,O_2}(\nu) + wT_{A,H_2O}(\nu) , \quad (4)$$

where w is the precipitable water vapor content in millimeters and the components T_{A,O_2} and T_{A,H_2O} are expressed in K and K mm^{-1}, respectively. The quantity w, and therefore the associated emission, is rapidly variable on timescales of minutes to hours. Simultaneous measurements at two frequencies ν_1 and ν_2 can be used to test the model with no need of an independent determination of w. In fact from equation (4) we can write

$$T_{A,atm}(\nu_1) = \beta + \alpha T_{A,atm}(\nu_2) , \quad (5)$$

where $\alpha = T_{A,H_2O}(\nu_1)/T_{A,H_2O}(\nu_2)$ is the slope and $\beta = T_{A,O_2}(\nu_1) - \alpha T_{A,O_2}(\nu_2)$ is the intercept of the expected linear correlation between the measured temperatures.

Variations in the atmospheric signal due to fluctuations in the water vapor column density have been measured and interpreted within the Kolmogorov turbulence model (Smoot et al. 1987b). Recently, Church (1995) has modeled the effects of water vapor variations on ground-based CMB anisotropy experiments with beam-switch and interferometric techniques.

3. MEASUREMENTS AND ERROR ANALYSIS

3.1. *Observational Technique*

We measured the atmospheric emission at 1.47, 2.0, 3.8, 7.5, 10, and 90 GHz, in three campaigns from WM (1986 July–August, 1987 August–September, and 1988 August–September) and in two campaigns from SP (1989 November–December and 1991 November–December). Some of these data (at 2.0, 3.8, and 7.5 GHz, and a small fraction of those at higher frequencies) were used to evaluate the atmospheric emission relevant for CMB absolute measurements. A summary of the radiometers and measurement campaigns is given in Table 1; details on each instrument can be found in the references listed in the last column.

The antenna temperature of the atmosphere, $T_{A,atm}$, was measured with zenith scans in which each radiometer repeatedly observed the sky at a set of zenith angles, Z. In general,

TABLE 1

RADIOMETER CHARACTERISTICS AND CAMPAIGNS OF ATMOSPHERIC MEASUREMENTS

ν (GHz)	λ (cm)	$\Delta\nu$ (MHz)	TYPE[a]	SENSITIVITY[b] (mK Hz$^{-1/2}$)	HPBW	$\langle f(0)\rangle$	CAMPAIGNS (Site and Year)	ZENITH ANGLES Z_1	ZENITH ANGLES Z_2	REFERENCE
1.47.....	21	200	TP	25	15° × 20°	1.027	SP 1991	0°	30°, 40°, 50°	1
2.0.....	15	200	TP	39	12 × 14	1.028	SP 1991	0	30, 40, 50	2
3.8.....	7.9	105	TP	18	16	1.041	WM 1986, 1987, 1988	0	30, 40	3, 4, 5
							SP 1989	0	30, 40	6
7.5.....	4.0	500	TP	62	20	1.026	WM 1988	0	30, 40	7
							SP 1989	0	30, 40	8
10.....	3.0	1000	D	46	12.5	1.015	WM 1986, 1987	0	30, 40, 47, 54	9, 5
90.....	0.33	2000	D	126	7.5	1.012	WM 1986, 1987, 1988	10, 20	50, 40	10, 5
							SP 1989	10, 20	50, 40	10

[a] TP = Total power receiver; D = Dicke receiver.

[b] Measured, 1 s integration time.

REFERENCES.—(1) Bensadoun et al. 1993; (2) Bersanelli et al. 1994; (3) De Amici et al. 1988; (4) De Amici et al. 1990; (5) Smoot et al. 1987a; (6) De Amici et al. 1991; (7) Kogut et al. 1990; (8) Levin et al. 1992; (9) Kogut et al. 1988; (10) Bersanelli et al. 1990.

© American Astronomical Society • Provided by the NASA Astrophysics Data System

1995ApJ...448....8B

TABLE 2

SUMMARY OF TYPICAL ERROR BUDGETS FOR $T_{A,atm}$[a]

Frequency (GHz)	Galactic Emission (K)	Ground Radiation (K)	Instrumental Effects (K)	Gain (K)	Pointing (K)	Beam Pattern (K)	Total Systematic (K)	Statistical Error (K)
1.47.....	0.171	0.014	0.047[b]	0.006	0.028	0.032	0.193[c]	0.027
2.0.....	0.081	0.014	0.035	0.006	0.014	0.026	0.094	0.014
3.8.....	0.023	0.035	0.029	0.020	0.005	0.019	0.058	0.004
7.5.....	0.010	0.041	0.013	0.004	0.007	0.014	0.047	0.037
10.....	0.019	0.025	...	0.012	0.006	0.025	0.041	0.034
90.....	<0.001	0.030	0.009	0.097	0.057	0.006	0.117	0.200

[a] Values reported are for pencil beam; errors at $\nu < 7.5$ GHz refer to SP, while at 7.5, 10, and 90 GHz they refer to WM.
[b] Extrapolated from vertical flip offset with an angle dependence.
[c] We have also considered a 0.061 K error for the RFI signal.

observations at two angles Z_1 and Z_2 produce an estimate of $T_{A,atm}$. The measured signal difference, $\Delta S_{Z_1/Z_2}$, is related to the atmospheric antenna temperature at zenith by

$$T_{A,atm,Z_1/Z_2}(0) \simeq \frac{G\Delta S_{Z_1/Z_2} - \Delta T_{Gal,Z_2/Z_2} - \delta T_{Z_1/Z_2}}{\langle f(Z_1)\rangle - \langle f(Z_2)\rangle} \langle f(0)\rangle , \quad (6)$$

where G is the radiometer gain constant, repeatedly measured during the experiment, and

$$\langle f(Z)\rangle = \int f(Z;\theta,\phi) g(\theta,\phi)\, d\Omega \quad (7)$$

is a convolution of the atmospheric air mass,[6] $f(Z)$, with the antenna gain pattern, g, when pointing the radiometer at a zenith angle Z. The quantity $\Delta T_{Gal,Z_1/Z_2}$ is the differential Galactic background component, which is subtracted based on low-frequency surveys (Haslam et al. 1982). The term $\delta T_{Z_1/Z_2}$ is the resultant of second-order, differential corrections due to ground radiation, angle-correlated instrumental effects, and possible radio-frequency interference (RFI):

$$\delta T_{Z_1/Z_2} = \delta T_{ground,Z_1/Z_2} + \delta T_{inst,Z_1/Z_2} + \delta T_{RFI,Z_1/Z_2} + \ldots . \quad (8)$$

Each known potential source of such effects is considered, and the size of the effect is measured with dedicated tests and/or evaluated with simulations.

In all of our measurements, except at 90 GHz,[7] we use $Z_1 = 0°$ (zenith) and a set of two or more tilt angles Z_2 in the range $30° < Z_2 < 55°$ (Table 1).

3.2. *Evaluation of Systematic Effects*

The relative importance of the various sources of uncertainty depends on frequency and site. In particular, at low frequencies the uncertainty is dominated by the subtraction of the large Galactic background through the propagation of the errors of the 408 MHz map (Haslam et al. 1982) used to evaluate the terms $\Delta T_{A,Gal,Z_1/Z_2}$ (Table 2). Systematic errors on $\Delta T_{A,Gal,Z_1/Z_2}$ are correlated between frequencies and could in principle affect the analysis of § 5.1; note, however, that at 90 GHz the correction is small ($\Delta T_{A,Gal,Z_1/Z_2} \lesssim 2$ mK).

We summarize in Table 2 the main systematic uncertainties and give typical values of the statistical errors. A detailed description of the typical sources of systematic effects can be found in the references listed in Table 1. From the present analysis the following additional points emerged.

In our 1986–1987 CMB measurements at 90 GHz (Bersanelli et al. 1989) we reported a slight (~2% level) but systematic asymmetry between evaluations of $T_{A,atm}$ from different angles. During the successive measurements (the WM 1988 and SP 1989 campaigns) the cause was identified with a slight discontinuity in the analog-to-digital converter (ADC) response near null voltage. The measured effect fully explains the observed asymmetry and produces corrections on $T_{A,atm}$(90 GHz) of up to ~0.1 K. The impact on the published value of T_{CMB} is negligible (<3 mK) since the effect cancels out at first order when subtracting $T_{A,atm}$ from the zenith antenna temperature. The other radiometers were not affected by this problem since their output voltages did not cross the discontinuity region of the ADC.

We have analyzed the 1.47 GHz atmospheric scans of the SP 1991 campaign and found RFI contamination at large zenith angles. Scans were performed with $Z_1 = 0°$ and $Z_2 = 30°$, 40°, and 50° over about 70% of the 24 hour right ascension. Our result is based on a small subset of these data ($1^h36^m < \text{R.A.} < 2^h16^m$ and $4^h3^m < \text{R.A.} < 5^h52^m$; $Z_2 = 30°$ and 40°) where the RFI is minimal and the differential Galactic background is reasonably low. Upper limits on possible RFI residual contamination results in an additional uncertainty of ±0.06 K on $T_{A,atm}$. No evidence of RFI was observed at the nearby frequency of 2 GHz (Bersanelli et al. 1994a) in the same campaign.[8]

4. RESULTS AND DISCUSSION

4.1. *Measured Atmospheric Antenna Temperatures*

Since each radiometer has a different beam pattern, the measurement results cannot be directly compared. We have corrected all the data for their specific value of $\langle f(Z)\rangle$, thus obtaining an homogeneous data set in terms of "pencil-beam" temperatures. Pencil-beam antenna temperatures will be assumed hereafter, for both data and models, unless otherwise stated.

Table 3 shows the results of the measurements of $T_{A,atm}$ from WM and SP, all taken with clear-sky conditions. As expected, the higher frequency results, and particularly those at 90 GHz, show strong intrinsic variations dominated by changes in the water vapor content. In Figure 1 we show the distribution of

[6] Accounting for the Earth's curvature, $f(Z) = (1 + r)/(\cos^2 Z + 2r + r^2)^{1/2}$, where r is the atmospheric height in units of Earth's radius. For small Z, $f(Z) \simeq \sec Z$.

[7] The 90 GHz Dicke radiometer had the input horns at a fixed 60° separation angle (Witebsky et al. 1986); see also Table 1.

[8] The 2 GHz radiometer had a front-end filter to prevent saturation of the first amplifier by out-of-band RFI signals.

© American Astronomical Society • Provided by the NASA Astrophysics Data System

1995ApJ...448....8B

TABLE 3

MEASURED[a] ATMOSPHERIC ANTENNA TEMPERATURE

	WHITE MOUNTAIN				SOUTH POLE		
FREQUENCY (GHz)	N^b	1986 (K)	1987 (K)	1988 (K)	N^b	1989 (K)	1991 (K)
1.47	...	...	...	...	120	...	0.840 ± 0.193
2.0	...	...	...	...	54	...	1.010 ± 0.095
3.8	248	0.835 ± 0.103	0.863 ± 0.061	0.917 ± 0.053	482	1.065 ± 0.058	...
7.5	312	...	...	1.055 ± 0.059	90	1.191 ± 0.062	...
10	184	1.01–1.27	1.07–1.23	...	...	...	...
90	386	9.4–17.5	8.4–16.0	7.0–16.1	349	8.4–10.3	...

[a] Pencil-beam values.
[b] Total number of atmospheric scans performed at each site.

the 90 GHz data from the two sites. The higher altitude of WM results in emission as low as $T_{A,\mathrm{atm}} \simeq 7$ K under favorable atmospheric conditions; on the other hand, at SP $T_{A,\mathrm{atm}} \simeq 9$ K, but the distribution is remarkably stable, much more than that from WM.

At low frequencies (3.8, 2.0, and 1.47 GHz) the water vapor contribution is negligible (e.g., from SP $wT_{A,\mathrm{H_2O}} < 3$ mK for $\nu < 4$ GHz). Values of $T_{A,\mathrm{atm}}$ reported in Table 3 are the averages (for $\nu \leq 7.5$ GHz) or ranges (for $\nu \geq 10$ GHz) of all the data in each campaign. Results from different years from WM are consistent within their error bars or fluctuation ranges. Figure 2 shows the measured values plotted together with the spectrum predicted for the two sites by the D&P model and shows the general consistency between experimental and theoretical results.

4.2. *Correlation of Simultaneous Data*

In the 1986 and 1987 campaigns from WM we collected extensive atmospheric measurements at 10 and 90 GHz, some of which were in coordinated simultaneous (or nearly simultaneous) scans. As shown in § 2, these can be used to test the atmospheric model. To set the appropriate simultaneity limit we fit equation (5) to the data at $\nu_1 = 10$ GHz and $\nu_2 = 90$ GHz taken in time windows of ±15 minutes (approximately the duration of a complete measurement) separated by varying intervals Δt. Table 4 reports the fit results and their quality in terms of χ^2/dof and r_S. The fit quality is preserved for $\Delta t = 30$ minutes (i.e., for data separated up to 45 minutes) and increasingly degrades for larger Δt. Thus we consider "simultaneous" all the data within ±45 minutes of each other. This is a measure of the timescale at which atmospheric variations at 10 and 90 GHz are coherent at the broad angular scale of our measurements.

The errors quoted in Table 4 include both statistical and systematic components. To properly account for the measurement errors in the fit we have decomposed the systematic uncertainties at the two frequencies, σ_ν, in a component, $\sigma_{\nu,p}$, proportional to $T_{A,\mathrm{atm}}$ and a component, $\sigma_{\nu,i}$, independent of $T_{A,\mathrm{atm}}$ such that $\sigma_\nu = (\sigma_{\nu,p}^2 + \sigma_{\nu,i}^2)^{1/2}$. In fact, only the com-

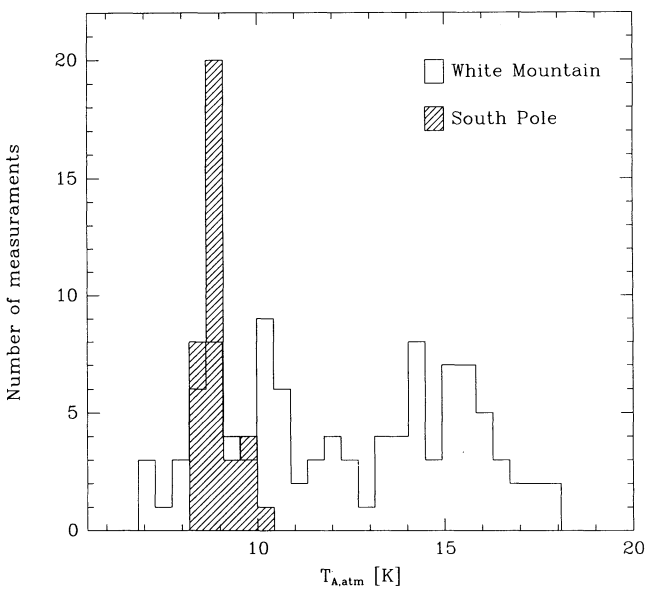

FIG. 1.—Distribution of $T_{A,\mathrm{atm}}$ at 90 GHz from SP (*dark area*) and WM (*white area*). The large scatter of the WM data reflects a real variation in the atmosphere. All the measurements were taken in clear-sky condtions.

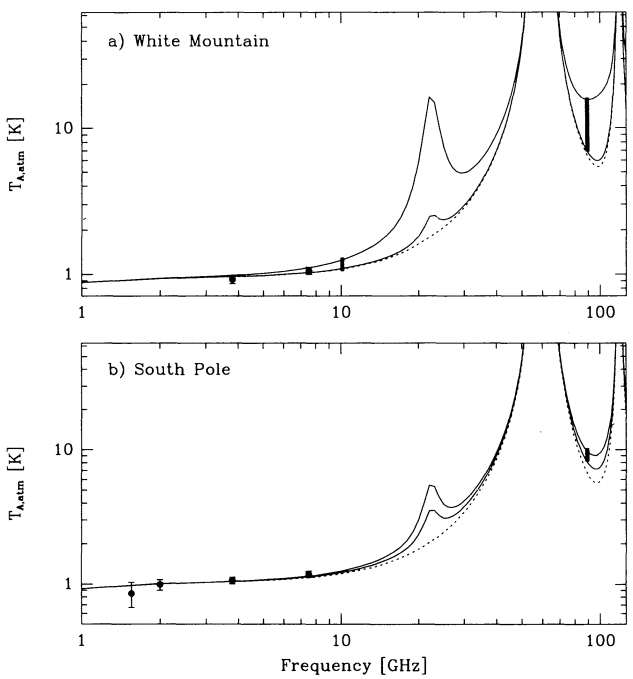

FIG. 2.—Measured and predicted atmospheric emission from WM and from SP. The dark vertical bars at 10 and 90 GHz represent the observed temperature ranges. The model spectrum is according to D&P. *Dashed line*, Dry atmosphere emission; *solid line*, total emission including water vapor contribution corresponding to $w = 0.2$–6 mm (WM) and $w = 0.5$–1.5 mm (SP).

© American Astronomical Society • Provided by the NASA Astrophysics Data System

1995ApJ...448....8B

TABLE 4

90/10 GHz CORRELATION: SIMULTANEITY CONDITION

Δt_{simult}	N	α	β (K)	χ^2_ν	r_S	CL
15 minutes	15	0.018 ± 0.003	0.961 ± 0.061	1.24	0.810	>99%
30 minutes	20	0.018 ± 0.003	0.956 ± 0.057	1.21	0.809	>99
45 minutes.....	23	0.016 ± 0.002	0.946 ± 0.057	1.79	0.807	>99
1 hr	29	0.016 ± 0.002	0.925 ± 0.062	2.85	0.804	>99
2 hr	28	0.015 ± 0.001	0.970 ± 0.053	3.90	0.795	>99
3 hr	23	0.016 ± 0.003	0.958 ± 0.065	4.85	0.733	>99
4 hr	13	0.011 ± 0.002	1.033 ± 0.071	8.66	0.637	98
5 hr	13	0.005 ± 0.003	1.116 ± 0.076	11.59	0.516	92

ponents $\sigma_{v,p}$ are relevant to the uncertainty on the slope α, while both $\sigma_{v,p}$ and $\sigma_{v,i}$ contribute to the uncertainty in β.

The simultaneous data are plotted in Figure 3. The high degree of correlation is evident; the Spearman rank correlation test yields $r_S = 0.81$ at the greater than 99.99% confidence level, and $\chi^2/\mathrm{dof} = 1.21$ (26 degrees of freedom). The best fit yields $\alpha = 0.018 \pm 0.002$ and $\beta = 0.958 \pm 0.058$ K. This is in excellent agreement with the predictions of the D&P adjusted model ($\alpha = 0.018$ and $\beta = 0.967$ K for frequencies 10 and 90 GHz).

Our results for the 10/90 GHz correlation, particularly for the slope α, differ significantly from the estimates based on the WM 1984 measurements, $\alpha = 0.028 \pm 0.003$ and $\beta = 0.82 \pm 0.14$ K (Costales et al. 1986). We note that the correlation in the Costales et al. data becomes evident only when including in the fit data taken with fog or clouds in the atmosphere. The different slope can be due to additional attenuation components from higher order terms and particularly absorption from liquid water droplets (Nilsson 1979). The high quality of the data presented here allows a precise correlation fit with only clear-sky data.

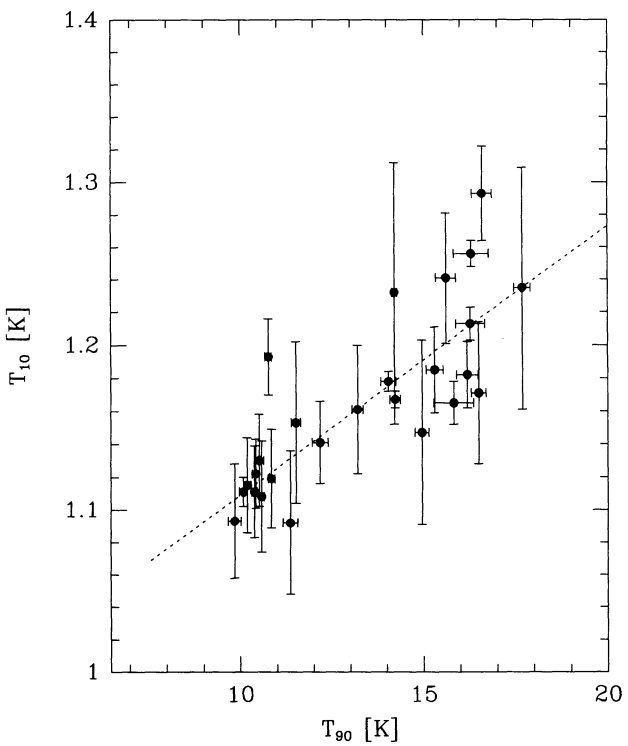

FIG. 3.—Simultaneous measurements at 10 and 90 GHz from WM (data from the 1986 and 1987 campaigns).

4.3. *Time-Variation Analysis*

To study the atmospheric variability we constructed the power spectrum of the atmospheric signal at the various frequencies. To account for the uneven sampling of the data we used a Lomb-Scargle algorithm (Press & Rybicki 1989). We show in Figure 4 the results for the 3.8, 7.5, and 90 GHz data from the SP 1989 campaign. As expected, at 90 GHz the signal variation level largely exceeds the radiometer noise. However, even at 3.8 GHz, where H_2O variations should be negligible, there is detection of a significant fluctuation component in the measured signal (Fig. 4*c*) at timescales of ~1 hr or more.

In order to verify the atmospheric nature of these fluctuations we have used the daily monitoring of atmospheric profiles carried out by the Meteorological Center of the Amundsen-Scott South Pole Station. Balloon probes were launched approximately every 12 hr providing profiles of pressure, physical temperature, and dew-point temperature up to 30 km altitude (the density scale heights of water vapor and oxygen are 2.2 and 9.5 km, respectively). We calculated the expected atmospheric emission with the D&P adjusted model for each measured profile at our observing frequencies of 3.8 and 90 GHz. Figures 5*a* and 5*b* (*top panels*) show the predicted values of $T_{A,\mathrm{atm}}$ together with the radiometric data taken within ±6 hr of the balloon measurements (i.e., excluding data taken when the meteo monitoring was occasionally interrupted). The agreement between data and modeled emission is remarkable. The Spearman correlation test of the radiometric data with the interpolated expected values yields $r_S = 0.7$ (≈ 99% confidence level) at 3.8 GHz and $r_S = 0.8$ (≈ 99% confidence level) at 90 GHz.

Figure 5*a* shows that the typical variation of $T_{A,\mathrm{atm}}$(3.8 GHz) is ~50–100 mK (i.e., up to ~10% of the emission). A peak variation of ~150 mK is predicted on November 29–December 1 by the D&P model with the measured atmospheric profiles.

The lower panels of Figure 5 show the O_2 and H_2O components in terms of lines and continuum contributions. The water vapor contribution at 3.8 GHz is expected to be negligible. The observed variations are over 2 orders of magnitude larger than what can be produced by any reasonable fluctuation of w. Oxygen line emission variations are also small (<5 mK), while the O_2 continuum dominates the observed variability. We verified that these variations are mainly determined by changes in the pressure profiles, while changes of the temperature profiles produce effects of order ~10 mK. We also note that the observed variations do not correlate with the

© American Astronomical Society • Provided by the NASA Astrophysics Data System

1995ApJ...448....8B

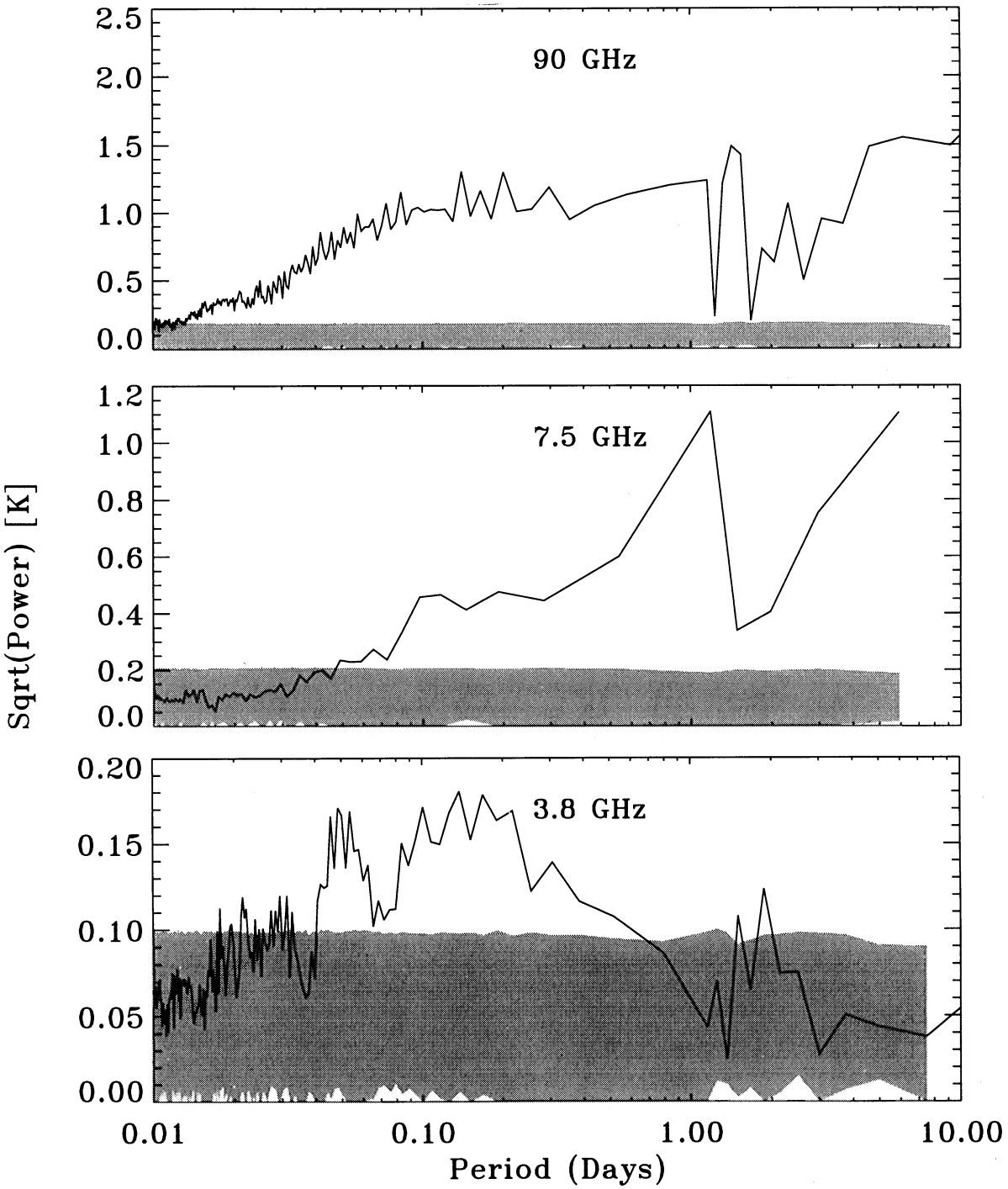

FIG. 4.—Power spectra of the measured signal at 3.8, 7.5, and 90 GHz (SP 1989). The gray area represent a Monte Carlo simulation of the (1 σ) radiometer noise.

atmospheric pressure at ground level (Fig. 6). Therefore a reliable model prediction of $T_{A,\mathrm{atm}}$ requires the complete atmospheric pressure profiles at the time of observation.

Large oxygen emission variations are also confirmed by the results at 90 GHz (Fig. 5*b*). Together with expected variations of $wT_{A,\mathrm{H_2O}}$ (as in the peak of December 8–9), strong features are to be ascribed to variations of O_2 emission driven by differences in the atmospheric pressure profile (up to $\Delta T \gtrsim 1$ K on November 30–December 2). Note that, unlike the 3.8 GHz case, at 90 GHz the dominant O_2 emission is the resonant component, due to the nearby line complex at $\nu \simeq$ GHz.

We conclude that the O_2 continuum emission undergoes variations at $\sim 10\%$ level due to the evolution of the atmospheric pressure profile on timescales of hours to days.

4.4. *Oxygen Continuum*

The low-frequency measurements can be used to check the model parameters which control the amplitude of the contin-

© American Astronomical Society • Provided by the NASA Astrophysics Data System

1995ApJ...448....8B

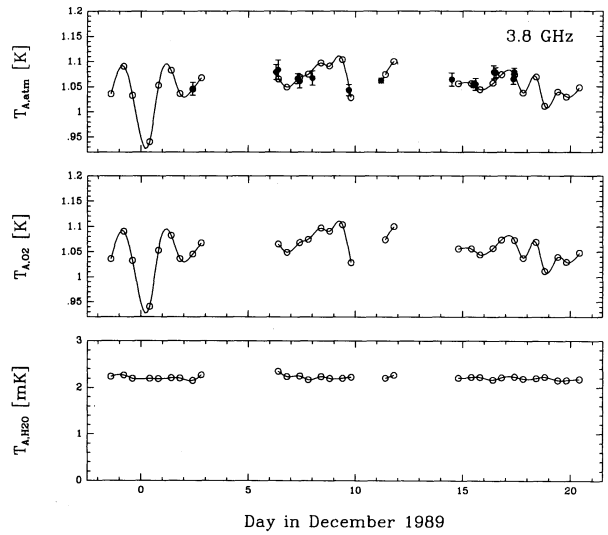

FIG. 5a

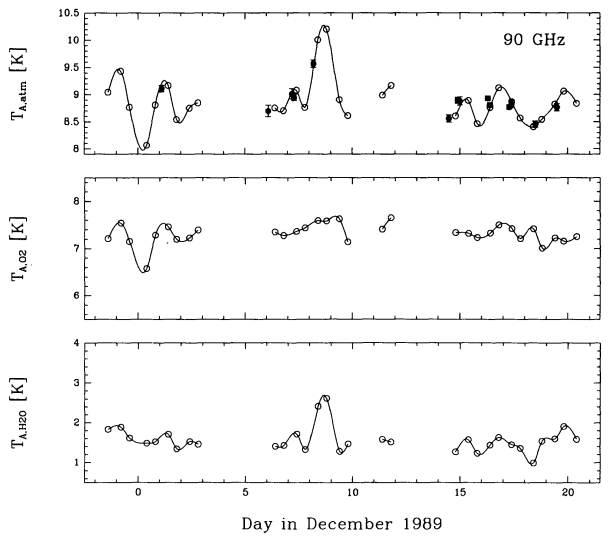

FIG. 5b

FIG. 5.—Measured and expected variations of the emission from the SP 1989 campaign: (*a*) 3.8 GHz; (*b*) 90 GHz. Theoretical evaluations are obtained with the D&P model using the daily local atmospheric profiles. Top panels show the total expected emission (*open circles interpolated by solid line*) and the measurements results (*filled circles with error bars*). Lower panels show the predicted variations of the oxygen (T_{A,O_2}) and water vapor (T_{A,H_2O}) components. Data taken more than 6 hr away from profile measurements or during heavy snowstorms have been excluded (see also Fig. 7).

uum O_2 emission. We subtract from the observed temperatures the minor components due to water vapor and O_2 line emission according to the D&P model. The residual oxygen nonresonant component, $T_{A,O_{2,c}}$, yields an estimate of the attenuation coefficient $(k_v)_{O_{2,c}}$ through equation (2), and hence an evaluation of the parameters *a* and *b* (eq. [3]). Since both θ and *b* are of order unity, the dependence of the antenna temperature on *b* is extremely weak. We fit our data using $b = 1.05 \pm 0.20$, a safe assumption based on previous determinations (D&P) and determine the parameter *a* implied by each measurement independently. To account for the O_2 variations described in § 4.3, we used the appropriate measured profiles θ and *p* when available, while for the other data we used average standard profiles. Table 5 summarizes the results. The errors in each evaluation of *a* are dominated by the measurement errors, with a component ± 0.0001 GHz kPa^{-1} due to the uncertainty in the *b*-parameter.

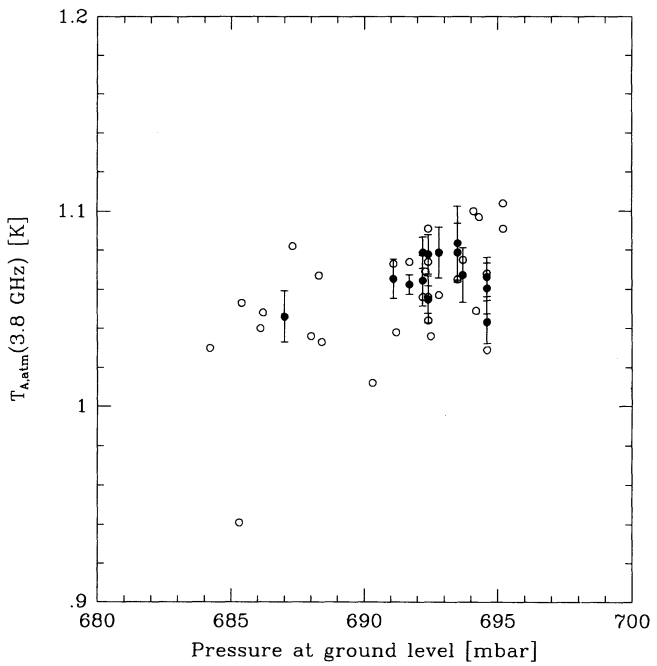

FIG. 6.—Atmospheric pressure at ground level vs. atmospheric antenna temperature at 3.8 GHz. Filled circles with error bars are measured values of $T_{A,atm}$(3.8 GHz); open circles are model predictions using the complete profiles. The lack of correlation is evident (using the measured data, for comparison with the results of § 4.3, we find $r_S = 0.1$ and CL = 15%).

The results derived from the two different sites, i.e., for significantly different profiles *p* and θ, are well consistent with each other. An overall weighted average yields $a = 0.00543 \pm 0.00017$ GHz kPa^{-1}, in good agreement with previous determinations (Kaufman 1967; Maryott & Birnbaum 1960) but with better accuracy. This result excludes values of *a* required by the assumptions of Lam (1977) and Smith (1981).

4.5. *Water Vapor Content*

The data at 90 GHz can be used to quantify water vapor content and variations. Model predictions for SP are $T_{A,O_2} \simeq 7.47$ K and $T_{A,H_2O} \simeq 1.58$ K mm^{-1}. With an observed temperature range $8.42 < T_{A,atm} < 10.39$ K this corresponds to precipitable water vapor values, *w*, between 0.5 and 1.8 mm. A similar comparison for WM data suggests typical values

TABLE 5

EVALUATIONS OF THE *a* PARAMETER[a]

Frequency (GHz)	*a* (WM) (GHz kPa^{-1})	*a* (SP) (GHz kPa^{-1})
1.47	...	0.00510 ± 0.00092
2.0	...	0.00526 ± 0.00054
3.8	0.00528 ± 0.00037	0.00536 ± 0.00035
7.5	0.00563 ± 0.00035	0.00553 ± 0.00037

[a] Values calculated with $b = 1.05 \pm 0.2$.

© American Astronomical Society • Provided by the NASA Astrophysics Data System

1995ApJ...448....8B

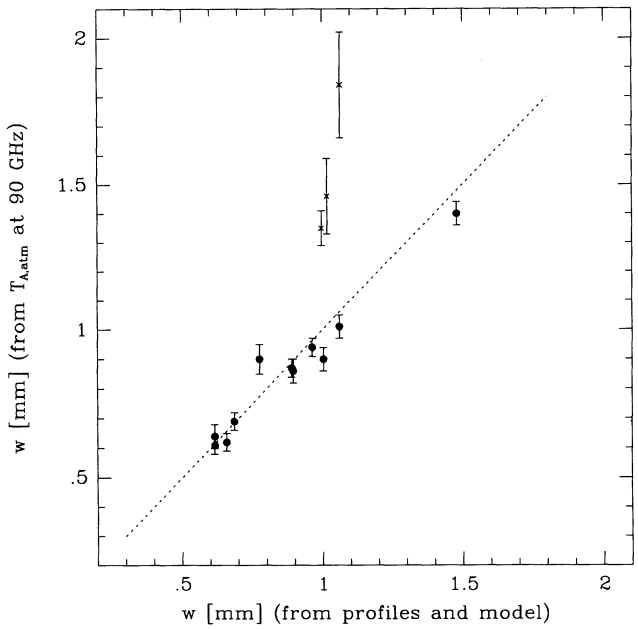

FIG. 7.—Correlation between water vapor content as deduced from the radiometric data and from the real-time dew-point temperature profiles from balloon probes (crosses indicate data taken during snowstorms).

$2 < w < 5$ mm over the three campaigns. A minimum $T_{A,atm} = 7.06$ K was observed on 1988 September 18, which directly sets an upper limit to the O_2 emission, predicted by the D&P model to be 6.80 K. This would correspond to water vapor content as low as $w \simeq 0.17$ mm. Note, however, that particularly low O_2 emission due to the pressure profile (§ 4.3) can concur to produce exceptionally low values of $T_{A,atm}$. Assuming a 10% drop of T_{A,O_2} we would get $w \simeq 0.6$ mm.

In the case of the SP 1989 campaign our results can more accurately test the model predictions since we can use the real-time monitoring of the local atmosphere. We estimate w from out $T_{A,atm}$ data accounting for the variable O_2 emission derived from the temperature and pressure profiles at the times of the observations. Then we convert the dew-point temperature profiles in relative humidity and thus estimate w independently of the radiometric measurements. The comparison in shown in Figure 7. The only three points that significantly deviate from the linear fit refer to radiometric measurements taken in the presence of ice crystals in the atmosphere, a common situation at SP. Excluding those points, the good agreement between the two estimates of w shows that the theoretical model successfully predicts the H_2O component at 90 GHz within the measurement errors. These values of w for the summer SP atmosphere are consistent with those reported by other groups with independent methods (Smyte & Jackson 1977; Pomerantz et al. 1984; Pajot et al. 1986; Meihnold et al. 1993), while the estimate of w by Dragovan et al. (1990) appears lower by about a factor of 2.

5. CONCLUSIONS

The comparison of our multifrequency measurements of the atmospheric emission with the D&P theoretical model is successful in both the high- and the low-frequency regimes and is cosistent for the two different observing sites. This confirms that future CMB absolute measurements can rely on model predictions, particularly at long wavelengths (≤ 10 cm), where direct measurements of $T_{A,atm}$ are subject to large uncertainties due to the subtraction of the strong Galactic background. However, if accuracies better than $\sim 10\%$ are required, real-time measurements of the evolution of pressure and temperature profiles are necessary to account for variations of T_{A,O_2} on timescales of hours to days. Monitoring of the ground-level atmospheric pressure does not provide sufficient information.

Past absolute measurements of the CMB at frequencies less than 10 GHz have assumed stable values of $T_{A,atm}$ in clear-sky conditions, based on the assumption that only changes in the water vapor column density, w, can produce significant variability. Our analysis provides a clue to some unexplained effects reported and discussed in previous works. Throughout our 3.8 and 7.5 GHz experiments (De Amici et al. 1988, 1990; Kogut et al. 1990; Levin et al. 1992) we observed atmospheric fluctuations greater than those expected from water vapor changes and radiometer noise alone, particularly when comparing independent sets of measurements. Similarly, excessive scatter in the CMB absolute calibration has sometimes been observed and attributed to instrumental effects (e.g., Levin et al. 1992; Kogut et al. 1990; Bersanelli et al. 1994a). Although pressure-driven O_2 variability might not explain all of the short-timescale variations, it certainly contributed to increase the overall spread of those data, with amplitudes up to 0.1 K. Another possible direct signature of atmospheric fluctuations due to pressure gradients on several-degree scales is the unexplained atmospheric drift pattern observed at 1.4 GHz by Staggs (1993) from a low-altitude site. We note also that if $T_{A,atm}$ and the absolute calibration are performed in narrow and separated time windows, the estimate of $T_{A,CMB}$ may be subject to a systemic error at the same amplitude level.

Extrapolations to low frequencies of simultaneous high-frequency measurements of $T_{A,atm}$, where T_{A,H_2O} is larger, are more complicated than previously thought. Accurate extrapolation requires multifrequency monitoring, since the H_2O and O_2 components are both variable and scale in very different ways with frequency. On the other hand, from dry, high-altitude sites T_{A,H_2O} is very small—below ~ 7–8 GHz; thus an effective way to extrapolate $T_{A,atm}$ in the Galactic-dominated low-frequency range is to perform simultaneous atmospheric scans at intermediate frequencies (~ 7 GHz), which would readily monitor the O_2 fluctuations.

Finally, we note that any small-scale pressure gradients present in the observed sky patch will produce temperature differences potentially affecting ground-based CMB anisotropy experiments. Our data are only sensitive to large angular scale pressure fluctuations (the scale of our measurements is 40°–60°) on timescales greater than a few hours. Pressure variations on smaller spatial scales are certainly present, although a quantitative estimate of their size is uncertain. A relatively direct comparison to our data is the careful discussion of Meinhold & Lubin (1991) and Meinhold et al. (1993) on their 90 GHz SP anisotropy experiment at degree resolution. They argue the presence of atmospheric regions with high and low pressure to explain observed residual drifts in their differential data. They assume 1% (70 mK) gradients of T_{A,O_2} on scales larger than the angular resolution, i.e., only $\sim 15\%$ of the typical daily variations we observed from the same site and at the same frequency (Fig. 5*b*). Although pressure gradients on degree-angular scales are probably smaller, it seems unlikely to expect them to be negligible at the extreme sensitivity level typical of anisotropy experiments. In order to

© American Astronomical Society • Provided by the NASA Astrophysics Data System

1995ApJ...448....8B

learn more about pressure-induced atmospheric variations at degree scales, multifrequency anisotropy studies correlated with accurate measurements of the atmospheric pressure and temperature profiles would need to be done at a number of different locations.

We thank the South Pole Meteorology Group for making readily available the atmospheric profile measurements. All members of the staffs and crews of the Amundsen-Scott Station and White Mountain Station always provided outstanding logistic support. We gratefully acknowledge the contribution of several people at various stages of the experiment, including J. Aymon, G. Bonelli, F. Cavaliere, J. Gibson, L. Levin, A. Passerini, G. Sironi, S. Tanaka, L. Tenorio, W. Vinje, and J. Yamada. This work has been supported by the US National Science Foundation under grant DPP 9018395, by the US Department of Energy under contract DE-AC3-76SF00098, by ENEA Progetto Antartide, by CNR-NATO Advanced Felloowship Program 215.24/02, and by EEC HCM contract CHRX-CT-920033.

REFERENCES

Ajello, C., Bonelli, G., & Sironi, G. 1995, ApJS, 96, 643
Bensadoun, M., Bersanelli, M., De Amici, G., Kogut, A., Levin, S. M., Limon, M., Smoot, G. F., & Witebsky, C. 1993, ApJ, 409, 1
Bersanelli, M., Witebsky, C., Bensadoun, M., De Amici, G., Kogut, A., Levin, S., & Smoot, G. F. 1989, ApJ, 339, 632
Bersanelli, M., Bensadoun, M., De Amici, G., Levin, S., Limon, M., Smoot, G. F., & Vinje, W. 1994a, ApJ, 424, 517
Bersanelli, M., et al. 1994b, in Present and Future of the Cosmic Microwave Background, ed. J. L. Sanz, E. Martinez-Gonzales, & L. Cayon (Berlin: Springer), 1
Costales, J., Smoot, G. F., Witebsky, C., De Amici, G., & Friedman, S. D. 1986, Radio Sci., 21, 47
Church, S. E. 1995, MNRAS, in press
Danese, L., & Partridge, R. B. 1989, ApJ, 342, 604 (D&P)
De Amici, G., Bensadoun, M., Bersanelli, M., Kogut, A., Levin, S., Smoot, G. F., & Witebsky, C. 1990, ApJ, 359, 291
De Amici, G., Bersanelli, M., Kogut, A., Levin, S., Limon, M., & Smoot, G. F. 1991, ApJ, 381, 341
De Amici, G., Smoot, G. F., Aymon, J., Bersanelli, M., Kogut, A., Levin, S., & Witebsky, C. 1988, ApJ, 329, 556
Dragovan, M., Stark, A. A., Pernic, R., & Pomerants, M. A. 1990, Appl. Opt., 29, 463
Gaier, T., Schuster, J., Gundersen, J., Koch, T., Seiffert, M., Meinhold, P., & Lubin, P. 1992, ApJ, 398, L1
Haslam, C. G. T., Salter, C. J., Stoffel, H., & Wilson, W. E. 1982, A&AS, 47, 1
Kaufman, I. A. 1967, Ph.D. thesis, Columbia Univ.
Kogut, A., Bensadoun, M., De Amici, G., Levin, S., Smoot, G. F., & Witebsky, C. 1990, ApJ, 355, 102
Lam, K. S. 1977, J. Quant. Spectrosc. Rad. Transf., 17, 335
Levin, S., Bensadoun, M., Bersanelli, M., De Amici, G., Kogut, A., Limon, M., & Smoot, G. F. 1992, ApJ, 396, 3
Liebe, H. J. 1981, Radio Sci., 16, 1183
———. 1984, Int. J. Infrared Millimeter Waves, 5, 207
Lubin, P. 1995, Astrophys. Lett. Comm., in press
Maryott, A. A., & Birnbaum, G. 1960, J. Chem. Phys., 32, 686
Meinhold, P., Chingcuanco, A., Gundersen, J., Schuster, J., Seifert, M., Lubin, P., Morris, D., & Villela, T. 1993, ApJ, 406, 12
Meinhold, P., & Lubin, P. 1991, ApJ, 370, L11
Nilsson, B. 1979, Appl. Opt., 18, 3457
Pajot, F., et al. 1986, in Proc. Space-Borne Sub-Millimeter Astronomy Mission, Segovia, Spain, June 4–6, 189
Partridge, R. B., et al. 1984, Phys. Rev. D, 29, 2683
Pomerantz, M. A., Pajot, F., Gispert, R., Lamarre, J. M., & Puget, J. L. 1984, Antarctic J. US, 19, 223
Press, W. H., & Rybicki, G. B. 1989, ApJ, 338, 277
Sironi, G., Bonelli, G., & Limon, M. 1991, ApJ, 378, 550
Smith, E. W. 1981, J. Chem. Phys., 74, 6658
Smyte, W. D., & Jackson, B. V. 1977, Appl. Opt., 16, 2041
Smoot, G. F., Bensadoun, M., Bersanelli, M., De Amici, G., Kogut, A., Levin, S., & Witebsky, C. 1987a, ApJ, 317, L45
Smoot, G. F., Levin, S., Kogut, A., De Amici, G., & Witebsky, C. 1987b, Radio Sci., 4, 421
Staggs, S. T. 1993, Ph.D. thesis, Princeton Univ.
US Standard Atmosphere. 1976, O-588-256 (Washington, DC: GPO)
Waters, J. W. 1976, in Method of Experimental Physics, ed. M. L. Meeks (New York: Academic), 12B, 142
Witebsky, C., Smoot, G. F., De Amici, G., & Friedman, S. D. 1986, ApJ, 310, 145

© American Astronomical Society • Provided by the NASA Astrophysics Data System